

RESEARCH ARTICLE

Numerical Analysis of Ion Flow in One-Bipole HVDC Transmission Line Using Revised Charge Injection Methods

MINHEE KIM¹ AND SE-HEE LEE² ¹Eco-Friendly Power Apparatus Research Center, Korea Electrotechnology Research Institute, Changwon 51543, South Korea²School of Electronic and Electrical Engineering, Kyungpook National University, Buk-gu, Daegu 41566, South Korea

Corresponding author: Se-Hee Lee (shlees@knu.ac.kr)

This work was supported by the Korea Institute of Energy Technology Evaluation and Planning (KETEP) funded by the Korean Government (MOTIE) under Grant 2022550000120.


ABSTRACT In the evolving field of electric power transmission networks, high-voltage direct current (HVDC) transmission has garnered attention for its efficacy in long-distance power delivery. However, HVDC systems are susceptible to corona discharges, which generate ions that disrupt the electric field distribution and pose safety concerns. To address these challenges, this study introduces new calculation techniques for predicting the electric field and ion current density around HVDC transmission lines using the finite-element method. The onset fields for the corona discharge were established at 14 and 13 kV/cm for positive and negative ions, respectively. Three novel techniques—average (A), cosine (C), and average–cosine combination (AC)—were introduced for continuous charge distribution. Additionally, an enhancement factor β was incorporated to reflect the various climatic conditions, enhancing the model's adaptability. This approach streamlines the analysis by reducing the reliance on complex parameters such as conductor roughness coefficient and climate constants. The techniques were validated across four different bundle configurations of transmission lines, with the AC technique demonstrating superior accuracy in predicting the electric field and ion current density, affirming its robustness in diverse scenarios, including under wind conditions. This research marks a significant advancement in modeling electrical discharge phenomena in HVDC environments, providing a simplified yet precise tool for ensuring electrical safety.

INDEX TERMS Corona discharge, HVDC, finite-element method, corona onset, charge injection.

I. INTRODUCTION

Recently, significant changes have happened in the electric power transmission network as a step toward power market growth and increases in energy deals [1], [2]. At the same time, the demand for long-distance transmission of high power to the city center grows as the number of power plants outside the city increases due to the increase in eco-friendly energy [1], [3].

In addition, high-voltage direct current (HVDC) transmission has attracted attention, which is advantageous for long-distance power transmission and for managing different grid-connected systems due to low power losses and

The associate editor coordinating the review of this manuscript and approving it for publication was Su Yan .

stability [4]. In contrast, ions are generated by corona discharges around a transmission line under HVDC environments due to the continuously applied unidirectional high voltage. These ions can distort the electric field distribution, and this additional electric field can be concentrated locally on the ground. Corona discharges can generate audible noise [5]. These corona discharges also cause energy loss, radio-frequency emission, and photon emission [6], [7], [8], [9], [10].

The electrical characteristics on the ground surface caused by transmission lines have significantly attracted research interest regarding electrical safety. In particular, the electric field strength and current density near the ground become important parameters for electrical environmental injury. In addition, the electric field affects obstructions such as

people and buildings with a wide range of conductivity and permittivity under the transmission line [11], [12]. Therefore, it is important to have a reliable analysis technique for evaluating the electric field and ion current density under the HVDC environment quickly and precisely.

Recently, several advanced methods have been developed for the simultaneous numerical calculation of the electric field and ion current density near the ground. These methods not only aim for precision but also strive for reduced computation time and enhanced efficiency, reflecting the evolving technological field [13]. The finite-element method (FEM) was initially proposed in 1979 by G.Cela [6], [7]. After the FEM was proposed, it was applied to different transmission line configurations to calculate changes in ion current density and electric field distribution considering the influence of wind in various climatic environments. There were also upstream FEM, adaptive FEM, SUPG-FEM, FE-FVM, and various other hybrid techniques that have been suggested with different modification techniques [8], [9], [10], [11], [12].

Most methods introduced so far probably show reasonable agreement with experimental results [13], [14]. In other words, even if the method of calculating the surface charge around the conductor changes, the electric field distribution on the ground cannot be practically altered much. That is why it is essential to compare the numerical analysis results with measurement data such as electric field and ion current density considering the various bundle configurations, with wind effect, etc., to verify the validity of the numerical model. Eventually, it is valuable to develop a numerical analysis model that can precisely predict the electric field and ion current density for various cases and flexibly respond to inclusive environmental variables.

In this study, we introduced a novel and practically universal method that adeptly characterizes the dynamic changes in ion current density and electric field surrounding transmission lines under high-voltage conditions. This method stands out for its real-time applicability and physical sensibility compared with traditional approaches. With the newly proposed method in this study, it is possible to solve inevitable problems, such as irregular oscillation and discontinuity, which can only occur when using the FEM. It also helps prevent the use of complicated parameters that include geometric and climatic conditions such as surface roughness factor, temperature, air pressure, humidity, and precipitation, including empirical dimensionless constants.

In this numerical analysis model, the onset fields in which the corona discharge starts around the conductor surface were set at 13 and 14 kV/cm [15]. In addition, for high numerical stability, the distribution of the generated charge by the corona discharge on the conductor surface was described using three techniques: average (A), cosine (C), and average–cosine combination (AC) techniques.

Furthermore, we proposed convenient and stable numerical methods that can reflect the environmental conditions for the corona discharge with the constant β categorized into three conditions: severe, ordinary, and moderate climate. This

indicates that the numerical analysis method was successfully verified based on various experimental results measured considering the transmission lines of various subconductor bundle configurations and two-directional wind.

II. CALCULATION METHODS

A. BASIC GOVERNING EQUATIONS

Under an HVDC transmission environment, transmission lines are sources of positive and negative ions. The generated ions mainly diffuse toward opposite polarity lines or the ground and the air. Some ions recombine with counterpart ions to become neutral. The additional electric field generated by corona discharge ions can be added to the initial electric field without space charge, increasing the electric field strength at the ground.

Equations (1)–(3) were employed in this study to analyze the electric field and ion current density under the HVDC transmission lines [5], [7], [16], [17]. Equation (1) is Poisson's equation which describes the relationship between the electric field and space charge generated by corona discharge ions. Equation (2) is the current continuity equation, including drift and diffusion for positive and negative ions. This equation also describes the change in ion current density in the analyzed area and the change in ion current density with time. Equation (3) describes the ion current density, including mobility, electric field, diffusion effect, and wind velocity.

$$\nabla^2 V = \frac{(\rho_+ + \rho_-)}{\epsilon_0} \quad (1)$$

$$\frac{\partial \rho_{\pm}}{\partial t} + \nabla \cdot \mathbf{J} = \frac{R\rho_+\rho_-}{e} \quad (2)$$

$$\mathbf{J}_{\pm} = \mp(\rho_{\pm}\mu_{\pm}\mathbf{E} + \rho_{\pm}\mathbf{W} - D\nabla\rho_{\pm}) \quad (3)$$

where ρ is the ion current density produced around the HVDC transmission line (C/m^3), \mathbf{E} is the electric field (V/m), ϵ_0 is the permittivity of vacuum (F/m), \mathbf{J} is the ion current density (A/m^2), D is the diffusion coefficient (m^2/s), R is the recombination coefficient (m^3/s), e is the elementary charge, \mathbf{W} is the wind velocity with direction (m/s), μ is the mobility of ions ($m^2/V\cdot s$), and the subscripts + and – relate to positive and negative ions, respectively. In this analysis model, the diffusion coefficient was set at $5 \times 10^{-6} m^2/s$. The mobility of positive ions was set at $1.3 \times 10^{-4} m^2/V\cdot s$, and the mobility of negative ions was set at $1.6 \times 10^{-4} m^2/V\cdot s$. The recombination coefficient was set at $1.6 \times 10^{-12} m^3/s$ [16], [17].

B. CHARGE INJECTION FUNCTIONS WITH ENHANCEMENT FACTOR

Most research has calculated the corona onset field, which is the electric field strength to initiate the corona discharge around the conductor, using Peek's law [18]. However, surface roughness factor, temperature, air pressure, humidity, and precipitation and even empirical dimensionless constants are needed to use this well-known method to derive the corona onset field [19], [20], [21]. Therefore, various numerical values have been suggested in previous research.

In this study, to prevent these numerical complexities, we set the corona onset field at a constant value suggested in CIGRE [15]. The corona onset fields were 14 and 13 kV/cm for positive and negative ions, respectively. These values were adjusted by considering the practical level by following the previous literature resulting from experimental results such as EPRI and CRIEPI. Equation (4) describes the corona onset voltage derived from Gauss’s law, and (5) indicates the initial surface charge around the conductor: [22].

$$V_c = E_c r \ln \frac{L}{r} \tag{4}$$

$$\rho_c = \frac{E_y}{E_c} \frac{8\epsilon_0 V_c (V - V_c)}{rLV(5 - 4V_c/V)} \times 10^7 \tag{5}$$

where E_c is the corona onset field (V/m), E_y is the electric field at the midpoint between two transmission lines in space charge-free state (V/m), V is the applied voltage (kV), and L is the distance between two lines (m). In (4) and (5), the initial surface charge around the conductor depends on the electric field at the surface. We introduced an electric field enhancement factor β to reduce the difficulty of complicated numerical modeling, including the surface condition of conductors and various climatic conditions, whether a corona discharge is more likely to occur or not. Finally, the corona charge initially generated from the conductor can be described as follows:

$$\rho_0 = \rho_c \frac{\beta E_{norm} - E_c}{\beta E_{max} - E_c} \quad (\beta |\vec{E}| \geq E_c) \tag{6}$$

$$\rho_0 = 0 \quad (\beta |\vec{E}| < E_c) \tag{7}$$

where E_{norm} is the electric field strength of the conductor (kV/cm), E_{max} is the maximum electric field strength of the conductor (kV/cm), and β is the electric field enhancement factor to adjust the surface charge and has a value of 0.6–3.

From the measurement results for the transmission line of 500 kV in [15], it is worth noting that the electric field on the ground varies significantly by 1.9 to 2.3 times during the harshest day, depending on the season or weather conditions, despite the line have the same conductor configuration. We observed a difference of 3.6 to 5 times in the ion current density. We adjusted the β to a broader range for the changing climate and environment. Under severe discharge conditions, where the corona discharge is more likely to occur, β has a bigger value to make corona discharge easily occur with increasing initial corona charge on the conductor surface. The changes in electric field and ion current density due to changes in β are described in more detail in section A of the IV validation cases.

III. SURFACE CHARGE DISTRIBUTION ON THE CONDUCTOR

A. NUMERICAL INSTABILITY DUE TO FINITE-ELEMENT DISCRETIZATION

Special theoretical approximations are not needed when employing the FEM to analyze the motion of ions around the transmission lines, unlike other calculation methods such as

integration, electric field line, and Gaussian tube [23], [24]. Considering the change in the electric field direction, the FEM makes it possible to calculate the ion current density and the deterioration of the electric field flexibly. However, an error can accumulate when using the FEM depending on the element division and matrix form with limited numerical space. Therefore, increasing the mesh for accuracy increases the overall calculation amount and reduces efficiency.

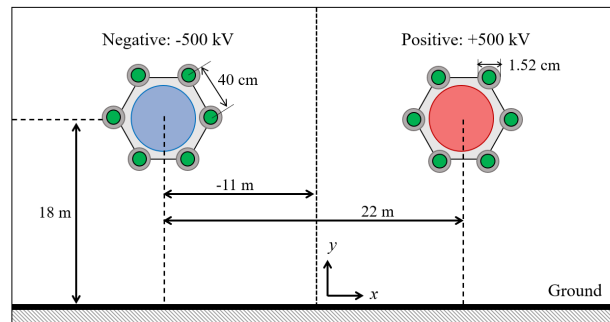


FIGURE 1. Configuration of the transmission line with 6-Bundle with ±500 kV for describing the FEM discretization.

To describe the instability due to FEM discretization, we initially numerically analyzed the ±500 kV transmission line with 6 bundles, as depicted in Fig. 1. As depicted in Fig. 2, a discontinuous region without a corona charge is formed on the surface of the conductor as the electric field strength is lowered after the corona discharge is generated. This phenomenon can happen in a lenient (languid, not severe, and lukewarm) environment where the corona discharge is not likely to occur. Because of this local corona non-occurring region on the conductor surface, there were inevitable irregular parts on the electric field and ion current density distribution at the ground, as depicted in Fig. 3.

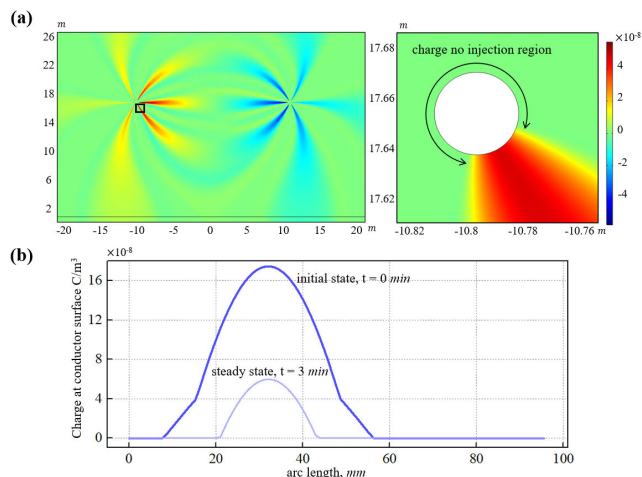


FIGURE 2. The space charge distribution has an inevitable discontinuous part caused by local corona non-occurring regions. (a) Space charge distribution around the transmission line and injection charge distribution around the subconductor. (b) Injection charge distribution by time.

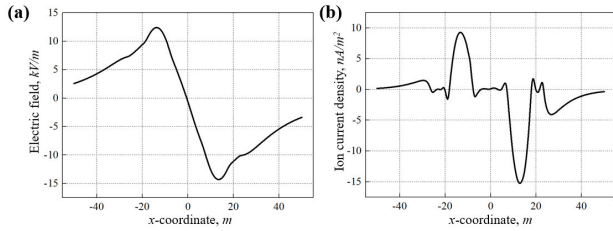


FIGURE 3. (a) Electric field and (b) ion current density under the transmission line on the ground. The abnormal region in the graphs is caused by the local corona nonoccurring region, as depicted in Fig. 1.

B. NEWLY SUGGESTED CHARGE INJECTION TECHNIQUES

As mentioned in the previous section, with the FEM, we introduced smoothing and continuous charge injection techniques for removing numerical instability. This instability due to FEM discretization could be released by integrating and continuously redistributing the corona charge on each sub-conductor. These techniques can be categorized into A, C, and AC techniques. Equations (8)–(10) describe the A, C, and AC techniques, respectively.

$$\rho_A = \frac{\oint \rho_0(\theta)Rd\theta}{\oint Rd\theta} \quad (\text{A technique}) \quad (8)$$

$$\rho_C(\theta) = \frac{\oint \rho_0(\theta)Rd\theta}{2} \cos\left(\frac{\theta}{2}\right) \quad (\text{C technique}) \quad (9)$$

$$\rho_{AC} = \frac{1}{2}(\rho_A + \rho_C) \quad (\text{AC technique}) \quad (10)$$

Every technique aims to numerically stabilize the calculation only by changing the distribution on the conductor surface, not the amount of total surface charge integrated over the conductor surface.

In (8), the A technique includes the meaning of the average value that distributes the surface charge around the sub-conductor uniformly. This value is calculated by integrating the total charge following the conductor surface generated by the corona discharge.

In (9), the C technique includes the meaning of a half-angle cosine value that reflects the charge distribution where the maximum charge density on the conductor surface is calculated from the original technique. This technique distributes the charge half-cosine function trigonometrically with the maximum value as the center point.

The A technique distributes the surface charge constantly over the conductor that cannot reflect the charge variation on the surface. The C technique somehow reflects the charge variation on the surface like the original technique, but still, there is one point on the conductor surface with zero charge. Therefore, in (10), the AC technique includes 50% of each A and C technique to the sum of two terms of the A and C techniques. Therefore, there is no charge-free region on the sub-conductor when using the AC technique due to the portion of the A technique.

Fig. 4 depicts the calculation results of the charge distribution around the sub-conductor when employing the original (O), A, C, and AC techniques. Herein, the O technique

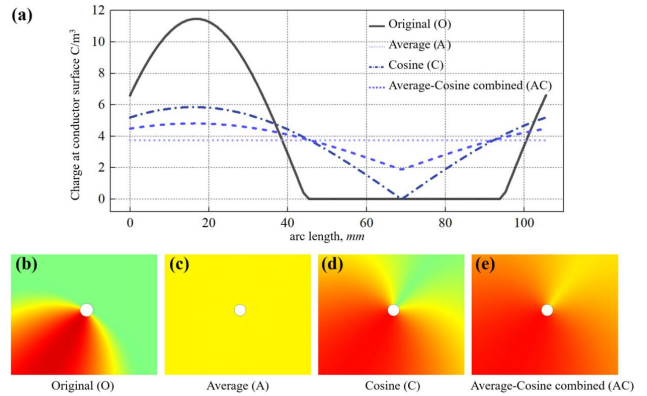


FIGURE 4. Charge distribution around the subconductor using the charge injection techniques. (a) Charge distributions calculated using all the techniques. Results when employing (b) the O technique, (c) the A technique, (d) the C technique, and (e) the AC technique.

refers to the calculated result without assumptions like (8)–(10). Fig. 4(a) shows a discontinuous region, a problem caused by the FEM while calculating the charge distribution on the conductor surface using the O technique. Fig. 4(b)–4(e) shows the charge distribution, which is radiated from a conductor, calculated using various techniques.

IV. VALIDATION CASES

In this study, we dealt with four kinds of validation cases, including various types of subconductors, the applied voltage, and the existence and nonexistence of wind. We validated our numerical analysis model by comparing each measurement data in previous research with the calculated results [15], [25], [26]. For the comparison of the measurement data and calculated results, we used cosine similarity, the distance between two data, and R^2 , the coefficient of determination.

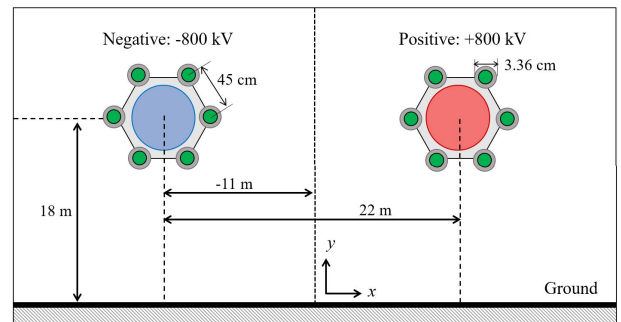


FIGURE 5. Configuration of the transmission line for validation case 1: 6-Bundle with ± 800 kV.

A. 6-BUNDLE WITH ± 800 kV

The validation case 1 is depicted in Fig. 5 [25]. The maximum electric field E_{max} on the conductor surface was 26.46 kV/cm and the E_y was 0.39 kV/cm when the space charge was not generated.

The experimental data can be divided into stages: top, average, and bottom. We compared these measurement data

with the results calculated using the A, C, and AC techniques. The results calculated using the three techniques showed greatly similar tendencies to the measurement data. The β values were 1, 0.86, and 0.68 from the top to the bottom value. In other words, the most severe conditions had the largest value of β , where the corona discharge occurred actively. In contrast, the lenient conditions had a relatively smaller β value, and the corona discharge rarely occurred.

To clarify the effect of changing β , the A technique was introduced, and the changes in electric field and ion current density were numerically analyzed according to three changes in β values: 0.68, 0.86, and 1. As shown in Fig 6, E_{\max} on the positive right side changed to 26.9 kV/m, 33.7 kV/m, and 36.6 kV/m, and ion current density changed to 32.6 nA/m², 60.1 nA/m², and 74.7 nA/m². The β value was adjusted in other validation cases to reflect the variation of each measurement value well better.

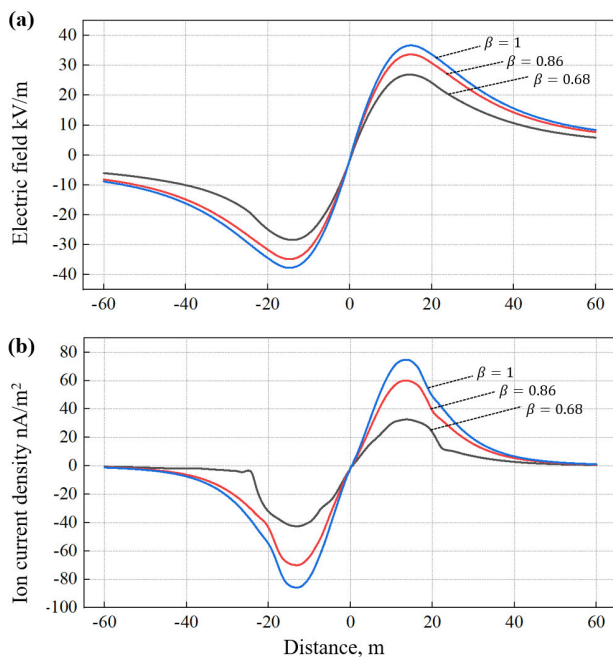


FIGURE 6. Numerical calculation results for varying β for 0.68, 0.86, and 1: (a) electric field distribution and (b) ion current density.

The calculation results of the A, C, and AC techniques were somehow well-fitted with the measurement data. As a logical conclusion, there are differences in the detailed morphology of the graphs, as depicted in Fig. 7. Fig. 7 shows the detailed numerical analysis results when β is 0.86. These differences would not stand out in the calculation results of the electric field distribution. In contrast, there are relatively remarkable differences in the ion current density. In Fig. 7, the A technique has the most alleviated shape.

The C technique has the maximum peak with a nonfinite concaved part, which was similar to the O technique in Fig. 3. The AC technique has the median value between the A technique in (8) and the C technique in (9). These three techniques proposed in this study demonstrate a higher concordance

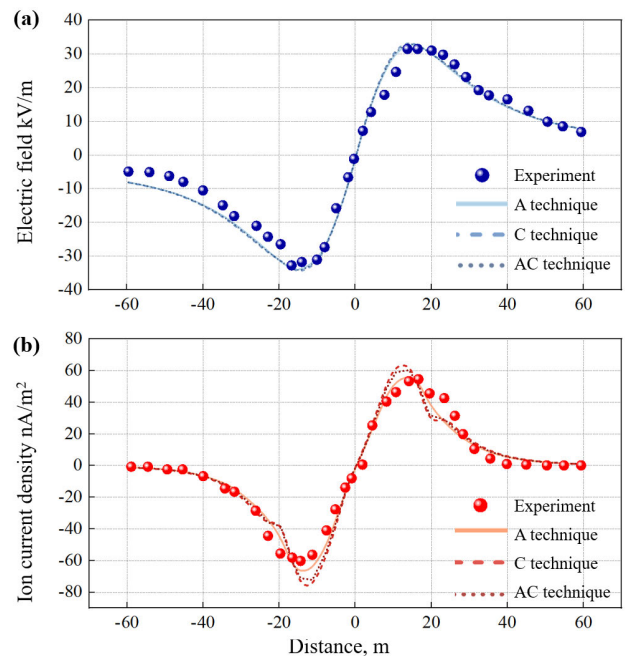


FIGURE 7. Three calculation results for β set at 0.86 with experimental values: (a) electric field distribution and (b) ion current density.

with the measurement data compared to the O technique. In fact, when quantifying the cosine similarity to the original experimental results using the R^2 value, the O technique yielded a value of 68%. In contrast, the other techniques all exceeded a value of 96%, indicating a significantly higher level of accuracy and reliability.

B. 2-BUNDLE WITH ± 500 kV

The validation case 2 is depicted in Fig. 8 [15]. The maximum electric field E_{\max} on the conductor surface was 25.56 kV/cm and the E_y was 0.31 kV/cm in the absence of space charge. The measurement data encompassed two conditions: a severe environment of the upper 5% and an average of 50%. The corresponding β was established for each condition. Notably, the data exhibited asymmetry on both the positive and negative sides. The β values ranged from 0.84 to 2.5 for the upper 5% and from 0.58 to 0.64 for the average 50%.

Fig. 9 depicts the electric field distribution and ion current density for the average 50% condition with a β value of 0.64 under severe circumstances. In Fig. 9(a), the electric field distribution of the O technique demonstrates a smaller peak value on the negative side compared to actual experimental data. Fig. 9(b) reveals a significant contrast in the ion current density distribution between the O and newly proposed techniques (A, C, and AC). Notably, the O technique displays regions where the charge does not reach the ground, resulting in an ion current density of zero and a considerably distorted distribution. Conversely, the A, C, and AC techniques show relatively smooth distributions, aligning more closely with experimental observations. In cases involving two bundles, the cosine similarity of the O technique

was approximately 61%, while the R^2 value was a mere 12%. Consequently, the A, C, and AC techniques demonstrate enhanced accuracy, as evidenced by their cosine similarity, the distance between data points, and the R^2 values.

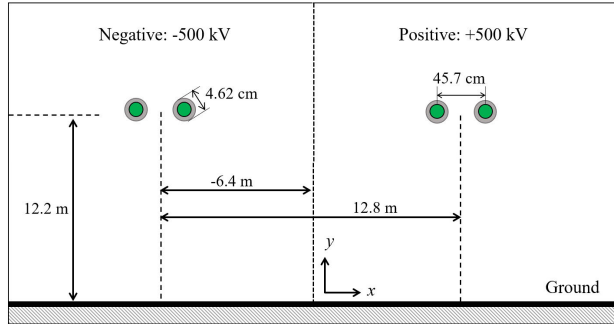


FIGURE 8. Configuration of the transmission line for validation case 2: 2-Bundle with ± 500 kV.

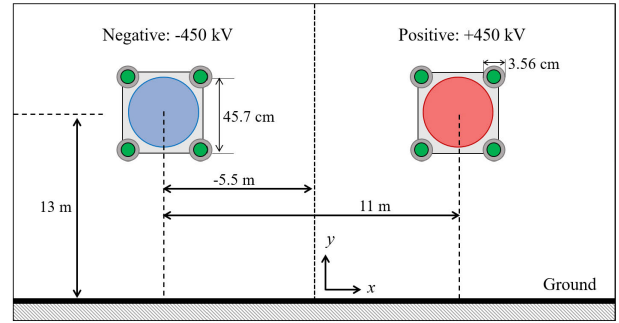


FIGURE 10. Configuration of the transmission line for validation case 3: 4-Bundle with ± 450 kV.

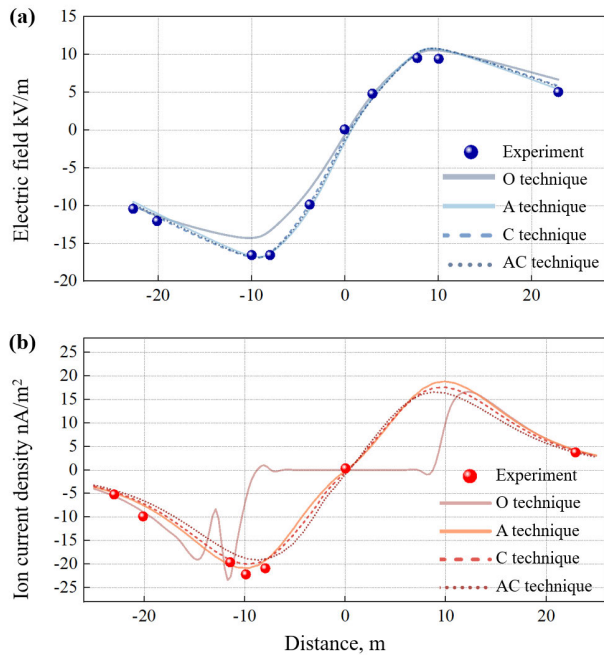


FIGURE 9. Three calculation results for β set at 0.64 with experimental values: (a) electric field distribution and (b) ion current density.

C. 4-BUNDLE WITH ± 450 kV

The validation case 3 is depicted in Fig. 10 [15]. The maximum electric field E_{max} on the conductor surface was 19.70 kV/cm and the E_y was 0.41 kV/cm when the space charge was not generated. The measurement data comprised two conditions: a severe environment of the upper 5% and an average of 50%. The β values were 0.98 and 0.845 for the upper 5% and the average 50%, respectively. The suggested A, C, and AC techniques have higher accuracy based on the cosine similarity, the distance between data, and the R^2 compared with the O technique.

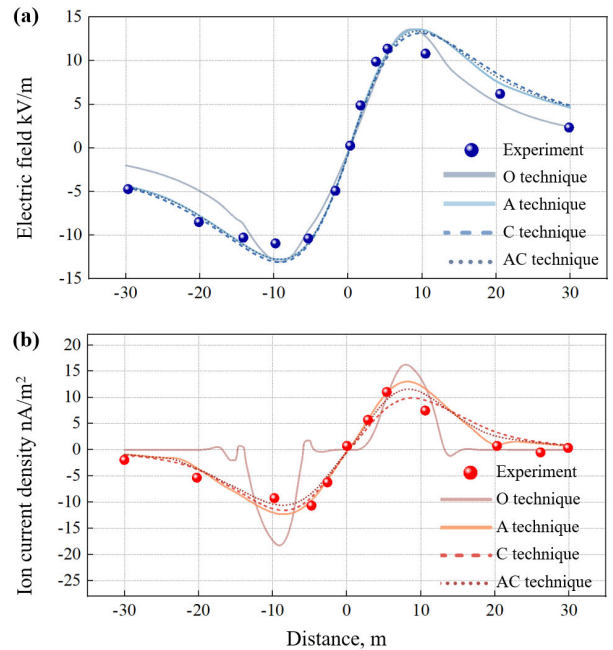


FIGURE 11. Three calculation results for β set at 0.845 with experimental values: (a) electric field distribution and (b) ion current density.

As depicted in Fig. 11(a), in particular, the O technique commonly has low accuracies for the electric field calculation results in a lenient (languid, not severe, and lukewarm) environment. For the cases in which the electric field on the conductor surface has an adjacent value of the corona onset field, i.e., 14 and 13 kV/cm for positive and negative ions, respectively, the discontinuously generated corona affects the calculation accuracy of the ion current density on the ground.

Fig. 11(b) describes the average 50% results of the ion current density when employing the suggested A, C, and AC techniques. With these techniques, the similarity can increase up to 94%, the distances between data decreased to 33%, and the R^2 increased to 93%. The most well-reflected technique was the AC technique when considering the similarities.

The newly proposed methods in this study were particularly effective in calculating the electric field strength and ion current density in the ground at an average of 50%. Furthermore, the usefulness and versatility of these proposed

methods were verified by comparing the calculation results of the ion current density and electric field on the ground with the measurement results.

D. 6-BUNDLE WITH ±900 kV INCLUDING WIND

The validation case 4 is depicted in Fig. 12 [26]. The maximum electric field E_{max} on the conductor surface was 29.15 kV/cm and the E_y was 0.20 kV/cm when the space charge was not generated.

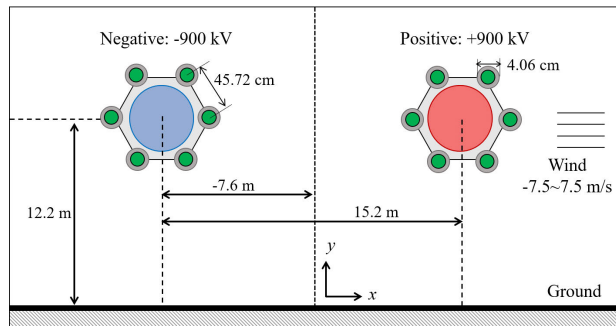


FIGURE 12. Configuration of the transmission line for validation case 4: 6-Bundle with ±900 kV employing varying wind strength.

The measurement data included the four cases with x -directional wind of -7.5 to -4.5 m/s, -4.5 to -1.5 m/s, -1.5 to 1.5 m/s, 1.5 to 4.5 m/s, and 4.5 to 7.5 m/s. By employing the proposed AC technique, which was validated in the previous validation cases, the calculation results of the ion current density describe the changing of the wind in Fig. 12.

The ion current densities calculated using the AC technique when considering the wind are indicated in Fig. 12. The maximum values of the electric field and ion current density moved parallel following the wind depending on the direction and strength of the wind. The tendencies of the measurement data were highly close to the numerical analysis results.

With a fully coupled method, we can analyze the ion behavior with the wind flow in real time which affects the electric field distribution based on the FEM.

V. DISCUSSION

The accuracy of the calculation results for the prior four cases, by applying the three newly proposed techniques, is detailed in Table 1 and Fig. 14. We meticulously accounted for the accurate best cases and the worst cases excluding the fourth case. Within the measurement environments, the total number of cases calculated for the electric field and ion current density on the ground was 14 (three conditions causing corona for case 1 and two for each of cases 2 and 3), and the accuracy was determined using three analytical indicators: similarity, distance, and R^2 . This resulted in a total of 42 cases, which were subsequently categorized into best accuracy and worst accuracy.

As depicted in Fig. 14, the three techniques proposed in this study significantly enhance the accuracy of the calculations when compared to traditional FEM approaches. Furthermore,

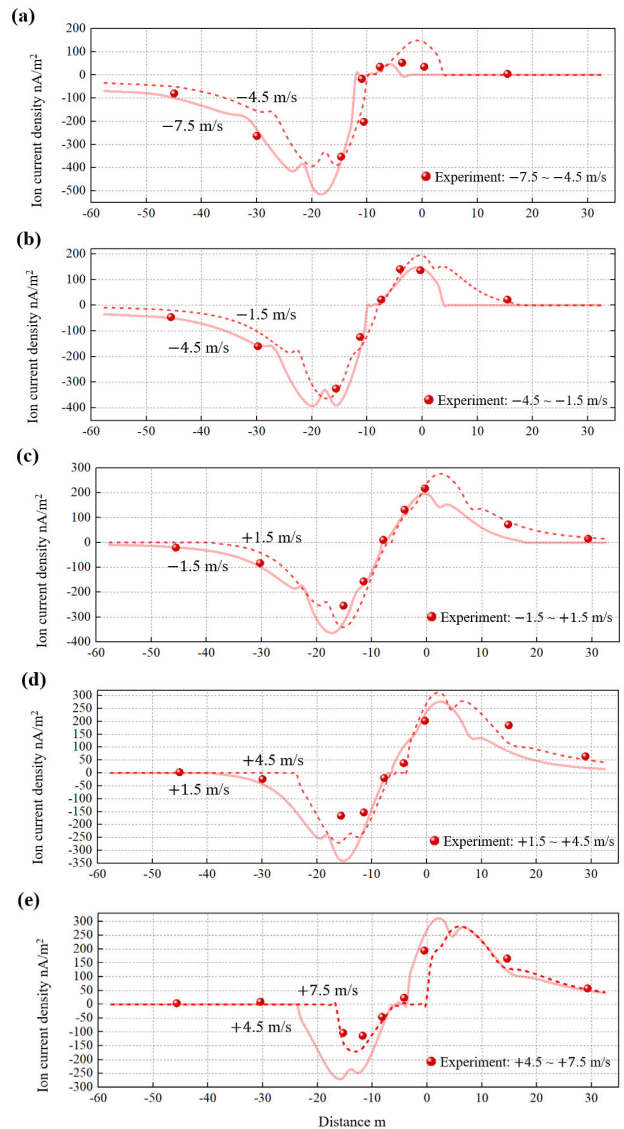


FIGURE 13. Calculation results of ion current density with experimental results for varying wind velocities: (a) -7.5 to -4.5 m/s, (b) -4.5 to -1.5 m/s, (c) -1.5 to $+1.5$ m/s, (d) $+1.5$ to $+4.5$ m/s, and (e) $+4.5$ to $+7.5$ m/s.

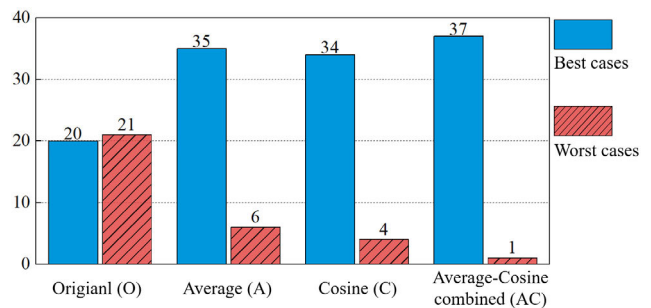


FIGURE 14. Performance analysis: best and worst cases for the four calculation techniques (O, A, C, and AC).

these methods consistently demonstrate high conformity with the measured data. Notably, the AC technique stands out,

TABLE 1. Number of best cases and worst cases.

Calculation Technique	Number of Best Cases			Total
	Case 1	CASE 2	CASE 3	
O (original)	8	7	5	20
A (average)	16	9	10	35
C (cosine)	11	11	12	34
AC (combined)	14	11	12	37

Calculation Technique	Number of Worst Cases			Total
	Case 1	CASE 2	CASE 3	
O (original)	10	4	7	21
A (average)	0	3	3	6
C (cosine)	3	1	0	4
AC (combined)	1	0	0	1

exhibiting only a single instance classified as the worst case, thereby providing highly accurate calculations of the ion current density and electric field for the validation cases.

VI. CONCLUSION

In this study, we addressed the discontinuities that originate from the FEM and introduced new numerical methods that enhance the accuracy of charge generation principles around conductors. Our numerical model was corroborated by comparison of four distinct measurement scenarios involving varying numbers of subconductors, applied voltages, and configurations specific to HVDC transmission lines. The salient findings are as follows.

- The corona inception electric fields were set at 14 and 13 kV/cm for the positive and negative ions, respectively.
- With conventional FEM-based calculation, there was a discontinuous problem in calculating the corona charge around the conductor surface for the case where the applied electric field is adjacent to the corona onset field. These discontinuous discharges around the conductor affected the calculation results of the electric field and ion current density on the ground.
- To overcome these problems, we proposed three methods to distribute the charge around the surface continuously without uninterrupted data, namely the A, C, and AC techniques.
- With the proposed calculation methods, we can minimize the complex values essential to calculate the initial charge, such as conductor roughness coefficient, climate constants for temperature and air pressure, and various empirical coefficients which have been suggested in previous research. As so, we described the most severe and relatively lenient conditions for the corona discharge by employing the field-enhancement factor β .
- We analyzed the four cases to validate the proposed methods, including wind conditions. To analyze the proposed methods' accuracy, we employed three different similarity calculation theories: the cosine similarity, the distance between data, and R^2 .

- The AC technique demonstrated superior accuracy across the 14 unique cases, as evidenced by the evaluation of the three similarity indicators.
- The newly suggested AC technique simplifies the calculation of ion current densities and electric fields, exceeding the capabilities of original methods from prior research. This research is expected to aid significantly in the prediction of electrical discharge phenomena on the ground across diverse environments, circumventing complex assumptions.

REFERENCES

- [1] A. Alassi, S. Ba nales, O. Ellabban, G. Adam, and C. MacIver, "HVDC transmission: Technology review, market trends and future outlook," *Renew. Sustain. Energy Rev.*, vol. 112, pp. 530–554, Sep. 2019.
- [2] R. Fu, P. Wei, G. Jiang, X. Zhou, Q. Wan, and G. Tang, "New market power driven multistage transmission expansion strategy in power markets," in *Proc. IEEE Power Eng. Soc. Gen. Meeting*, Jun. 2006, p. 8.
- [3] H. Wang and M. A. Redfern, "The advantages and disadvantages of using HVDC to interconnect AC networks," in *Proc. 45th Int. Universities Power Eng. Conf.*, Aug. 2010, pp. 1–5.
- [4] B. R. Andersen, "HVDC transmission-opportunities and challenges," in *Proc. 8th IEE Int. Conf. AC DC Power Transmiss.*, Mar. 2006, pp. 24–29.
- [5] B. Zhang, J. Mo, and J. Liu, "Calculation of ion flow fields of HVDC transmission lines by coupling flux tracing method with finite element method," in *Proc. IEEE Int. Conf. High Voltage Eng. Appl.*, Sep. 2020, pp. 1–4.
- [6] X. Zhang, I. Cotton, S. M. Rowland, Q. Li, C. Lian, W. Li, and C. Plaengraphan, "Audible noise and corona discharge from water droplets on superhydrophobic HVAC conductors," *IEEE Trans. Power Del.*, vol. 38, no. 6, pp. 3771–3781, Dec. 2023.
- [7] Y. Yi, Z. Chen, W. Tang, and L. Wang, "Calculation of ion flow environment of DC transmission lines in the presence of charged aerosol particulates based on upwind-FEM," *Electric Power Syst. Res.*, vol. 184, Jul. 2020, Art. no. 106289.
- [8] W. Janischewskyj and G. Cela, "Finite element solution for electric fields of coronating DC transmission lines," *IEEE Trans. Power App. Syst.*, vol. PAS-98, no. 3, pp. 1000–1012, May 1979.
- [9] T. Takuma and T. Kawamoto, "A very stable calculation method for ion flow field of HVDC transmission lines," *IEEE Trans. Power Del.*, vol. PD-2, no. 1, pp. 189–198, Jan. 1987.
- [10] Z. Al-Hamouz, M. Abdel-Salam, and A. Mufti, "Improved calculation of finite element analysis of bipolar corona including ion diffusion," in *Proc. IEEE Ind. Appl. Conf., 31st IAS Annu. Meeting*, Oct. 1996, pp. 1912–1918.
- [11] J. Liu, J. Zou, J. Tian, and J. Yuan, "Analysis of electric field, ion flow density, and corona loss of same-tower double-circuit HVDC lines using improved FEM," *IEEE Trans. Power Del.*, vol. 24, no. 1, pp. 482–483, Jan. 2009.
- [12] Z. Luo, X. Cui, and J. Lu, "Analysis of ionized field under HVDC transmission lines with buildings nearby," in *Proc. Asia-Pacific Int. Symp. Electromagn. Compat.*, Apr. 2010, pp. 277–280.
- [13] Y. Liu, Z. Li, B. Wan, L. Zhang, H. Yuan, and J. Lai, "Research on calculated method for space electric field around HVDC transmission lines with buildings nearby," *IET Gener., Transmiss. Distrib.*, vol. 16, no. 17, pp. 3363–3373, Sep. 2022.
- [14] J.-H. Kim, S. Joo, and Y.-S. Chung, "Improved flux tracing method based on parametric curve for calculating ion flow field of HVDC transmission lines," *IEEE Access*, vol. 9, pp. 105724–105732, 2021.
- [15] J. A. Jardini, B. Bisewski, B. Zhang, C. A. Peixoto, D. Renew, D. Lee, E. Aranda, G. Johnson, H. Hammarsten, J. F. Nolasco, and J. Lundquist, "Electric field and ion current environment of HVDC overhead transmission lines," Int. Council Large Electr. Syst., Paris, France, Tech. Brochure 473, 2011.
- [16] Y. Park, R. K. Jha, C. Park, S.-B. Rhee, J.-H. Lee, C.-G. Park, and S.-H. Lee, "Fully coupled finite element analysis for ion flow field under HVDC transmission lines employing field enhancement factor," *IEEE Trans. Power Del.*, vol. 33, no. 6, pp. 2856–2863, Dec. 2018.

- [17] A. M. Sayed, A. M. Ahmad, S. A. Ward, and E. M. Shaalan, "Improved prediction of ion mobility for precipitators using FDM-FMG on fine computational domains," *Electric Power Syst. Res.*, vol. 214, Jan. 2023, Art. no. 108833.
- [18] J. Qiao, J. Zou, and B. Li, "Calculation of the ionised field and the corona losses of high-voltage direct current transmission lines using a finite-difference-based flux tracing method," *IET Gener., Transmiss. Distrib.*, vol. 9, no. 4, pp. 348–357, Mar. 2015.
- [19] F. W. Peek, *Dielectric Phenomena in High-Voltage Engineering*. New York, NY, USA: McGraw-Hill, 1929.
- [20] Y. Zebboudj and R. Ikene, "Positive corona inception in HVDC configurations under variable air density and humidity conditions," *Eur. Phys. J. Appl. Phys.*, vol. 10, no. 3, pp. 211–218, Jun. 2000.
- [21] L. Min, L. Lei, L. Bin, G. Chao, L. Tianwei, Y. Zhanqing, F. Yin, and D. Mengting, "Prediction method on corona inception field intensity for HVDC fittings in high altitude area," in *Proc. IEEE Int. Conf. High Voltage Eng. Appl. (ICHVE)*, Sep. 2016, pp. 1–5.
- [22] Z. Shiling, "Theory and experimental study of corona initial E-field strength of HVDC large fittings," *J. Phys., Conf.*, vol. 1750, no. 1, Jan. 2021, Art. no. 012085.
- [23] M. Abdel-Salam and Z. Al-Hamouz, "A finite-element analysis of bipolar ionized field," *IEEE Trans. Ind. Appl.*, vol. 31, no. 3, pp. 477–483, Jun. 1995.
- [24] S. Fortin, H. Zhao, J. Ma, and F. P. Dawalibi, "A new approach to calculate the ionized field of HVDC transmission lines in the space and on the earth surface," in *Proc. Int. Conf. Power Syst. Technol.*, Oct. 2006, pp. 1–7.
- [25] H. Zhao, S. Fortin, and F. P. Dawalibi, "Distortion of the potential around HVDC transmission lines caused by corona space charge," in *Proc. Asia-Pacific Power Energy Eng. Conf.*, Mar. 2009, pp. 1–4.
- [26] J. Qiao, J. Zou, J. Yuan, J. Lee, and M. Ju, "Method of local characteristics for calculating electric field and ion current of HVDC transmission lines with transverse wind," *IET Gener., Transmiss. Distrib.*, vol. 11, no. 4, pp. 1055–1062, Mar. 2017.



space charge dynamics, polymeric insulators, and interface phenomena at hetero-dielectric insulators.

MINHEE KIM received the B.S. degree in physics from Sungkyunkwan University, Suwon, South Korea, in 2012, and the M.S. and Ph.D. degrees in electrical engineering from Kyungpook National University, Daegu, South Korea, in 2019 and 2022, respectively. She is currently doing her research with the Korea Electrotechnology Institute (KERI), South Korea. Her research interests include the numerical analysis of dielectric breakdown, high voltage, electric discharge,



of Electrical Engineering, Kyungpook National University, in 2008. His research interest includes analysis and design for electromagnetic multi-physics problems spanning the macro- to the nano-scales.

SE-HEE LEE received the B.S. and M.S. degrees in electrical engineering from Soongsil University, Seoul, South Korea, in 1996 and 1998, respectively, and the Ph.D. degree in electrical and computer engineering from Sungkyunkwan University, Suwon, South Korea, in 2002. He performed his postdoctoral research with the Massachusetts Institute of Technology (MIT) and the Korea Electrotechnology Research Institute (KERI), before joining as a Faculty Member of the Department

• • •